Supplementary Information

Table of Contents

1. Materials and Methods

Reagents. All solutions were made using DNAse/protease-free water purchased from FisherScientific. Synthesized oligonucleotides were obtained from Integrated DNA Technologies, Inc (Coralville, IA) and concentrations of oligonucleotide stock solutions were quantified via absorbance at 260 nm on a ThermoScientific NanoDrop One (Waltham, MA).

Annealing of DNA Tiles. All tiles were annealed in 1 mL microcentrifuge tubes overnight (~8-10 h) in a 2 L bath of water after being heated to 95 ^{o}C and boiled for 5 min. Oligonucleotides were combined in a total volume of 1 mL with a concentration of 100 nM. Unless otherwise specified, tiles were annealed with variations of T1, T2, T3, and T4, but not the P-strand, hybridization buffer 1: 50 mM Tris-HCl, 50 mM $MgCl_2$, 0.1% Tween-20, and pH 7.4.

Melt Curve Fluorescence Assays. Using DNA tiles previously annealed, UMB and ROX were added to the solutions to a final concentration of 25 nM and P-strand was added to a final concentration of 200 nM. Bringing the total volume to 30 µL each using either water or analyte, the samples were then added to the 96-well plate. A control consisting of only UMB and ROX were used, in addition to a sample containing the tile with no P-strand added, and a sample with no analyte added.

After adding the samples to the plate, an optical adhesive cover was securely fitted to the top of the plate and wells were sealed using a tool provided with the QuantStudio™ 6 Flex System. The plate was lightly flicked to eliminate bubbles and was vortexed and centrifuged for 20 s on a Fisher Scientific Mini Plate Spinner Centrifuge (Hampton, NH). After allowing 30 min for annealing the plate was then placed into the QuantStudio™ Flex 6 system and cooled to 5 ^{o}C where it was held for 5 min. The fluorescence of the samples was then read continuously as the samples were heated from 5 ^{o}C to 70 ^{o}C (0.1 ^{o}C/s). ROX was selected as a passive reference and FAM™ was read as the 'Target'. Although the system was calibrated to account for well factors, background, and dye fluorescence, there were small variations between the background fluorescence of UMB and controls without analyte; therefore, there may be small fluorescence value variations observed depending on the date of the experiment.

Data was exported to excel and subsequently to OriginLab 2021 (Northampton, MA) for data normalization and processing. The processed readings from at least three wells were averaged and plotted as a function of F_{FAM}/F_{ROX}. The derivative of fluorescence vs time was calculated by the QuantStudio™ Real-Time PCR Software to determine the melting temperature (T_m).

Limit of Detection. The limit of detection was determined for each study by conducting fluorescence experiments using a 60 µL quartz cuvette in a PerkinElmer (San Jose, CA) LS-55 Fluorescence Spectrophotometer with a xenon lamp. (λ_{ex} = 485 nm, λ_{em} = 517 nm). The samples were used directly from annealed tiles, and, to this solution, P-strand was added such that the final concentration was 200 nM and UMB was added to a final concentration of 25 nM. After the addition of analyte at varying concentrations, the samples were incubated in a 24 ^{o}C water bath for 30 min before being taken out of the bath and analyzed. Fluorescent values at 517 nm were recorded for three independent trials for each sample. The averages and standard deviations were plotted in Excel and OriginLab 2021 (Northampton, MA) and the linear region was found and fitted with an equation. The LOD was determined by using the equation with the fluorescent signal of the blank + 3*(Standard deviation of the blank).

Differentiation Fluorescent Assays. The differentiation of each tested sensor was determined by conducting fluorescence experiments in a similar manner to the limit of detection. For the OWL1 design, the samples were made such that R_x and P_y were added to final concentrations of 150 nM and 200 nM, respectively, unless stated otherwise. The differentiation factor ($D_f = 1- \Delta F_{mm}/\Delta F_m$) was calculated with ΔF representing the difference in signal from the blank for the mismatched (mm) and matched (m) analyte, respectively, and subtracting this from 1. For the F_m/F_{mm} assays, this was calculated by taking the Fluorescence of the Wild-Type analyte (F_m) and dividing it by the Fluorescence of the respective SNV-containing analyte corrected by the blank. All calculations were done using the fluorescent average of at least three trials.

Kinetics Assays. Using the same experimental conditions as for the other fluorescent assays, the fluorescence was measured over 45 min on a Cary Agilent Fluorimeter for 45 min. The OWL2 sensor and P-strand were mixed, and analyte was added, and fluorescence was read immediately afterwards.

Table S2. Oligonucleotides used for the assembly of the OWL2 Sensor variations

Name	***Sequence 5'-> 3'***
UMB	F-CG C GTTC CCATA CAAC CAATC GCG-BQ1
T1	GTA TCA GTC ATT ACC AGT AGT CGGAC CTAGG CTCTCGGT CTA G CCAC TTAAC
$T2_2$	ACT ACT GGT AAT GAC TGA TAC *ttt* C GGC GCA TGG GAC GTG
$T3_2$-9 no linker	CCTAG GTCCG GAACG TGA AGG TACT TATGG
$T3_2$-9-ttt	CCTAG GTCCG *ttt* GAACG T GAA GGT ACT TATGG
$T3_2$-9 iSp18	CCTAG GTCCG/*iSp18*/ GAACG TGA AGG TACT TATGG
$T3_2$-9 RiSp18	CCTAG GTCCG *ttt* GAACG T */iSp18/* GAA GGT ACT TATGG
$T4_2$	GC CTC CCG GGA CGT GT ttt GTT AA GTGG CTAG ACCGAGAG
$T3_2$-9 + $T4_2$+1	CGC CTC CCG GGA CGT GT ttt GTT AA GTGG CTAG ACCGAGAG CCTAG GTCCG ttt GAACG T GAA GGT ACT TATGG
$T4_2$+1	CGC CTC CCG GGA CGT GT ttt GTT AA GTGG CTAG ACCGAGAG
$T4_2$-1	C CTC CCG GGA CGT GT ttt GTT AA GTGG CTAG ACCGAGAG
CT2	ACT ACT GGT AAT GAC TGA TAC ttt GTTC AAGA AATT CAAC
CT3-9	CCTAG GTCCG ttt GAACG TCCAG GCAGC TATGG
CT4	ACTT CTCC TGCT AGAA ttt GTT AA GTGG CTAG ACCGAGAG
CT4+1	AACTT CTCC TGCT AGAA ttt GTT AA GTGG CTAG ACCGAGAG

F, fluorescein; BQ1, black hole quencher 1; underlined are the fragments complementary to UMB probe; ttt, trithymidine linkers between tile-forming fragments and the analyte binding arms; /*iSp18*/ internal spacer 18.

Table S3. Sequences of P-strand and R-strand variations used in this study

Name	***Sequence 5' -> 3'***
P^{9}_{9}	GTTG CAC ACT GCC GATTG
P^{8}_{9}	GTTG CAC ACT GCC ATTG
P^{9}_{8}	GTTG CAC ACT GC GATTG
P^{9}_{8} A>G	GTTG CAC GCT GC GATTG
P^{9}_{8} C>T	GTTG CAC ATT GC GATTG
P^{10}_{8}	GGTTG CAC ACT GC CGATT
P^{10}_{9}	GGTTG CAC ACT GCC CGATT
P^{8}_{8}	GTTG CAC ACT GC ATTG
P^{9}_{7}	GTTG CAC ACT G GATTG
C^{9}_{8}	GATTG GTTG CAC ACT GC
CP^{9}_{9}	GTTG AGTA AACGA GATTG
CP^{9}_{8}	GTTG AGTA AACG GATTG
R^{10}_{10}	GAACG GTGAAGGTAC TATGG

Nucleotides complementary to SNV sites are in red; Underlined are the fragments complementary to UMB probe

Table S4. Sequences of the analytes used in this study

Name	***Sequence 5'-> 3'***
Tau60-WT	CA AAC ACG TCC CGG GAG GC G GCA GTG TGA GTA CCT TCA C AC GTC CCA TGC GCC GTG CTG T
Tau60-WT (RNA)	ca aac acg ucc cgg gag gc g gca gug uga gua ccu uca c ac guc cca ugc gcc gug cug u
Tau60-0C	CA AAC ACG TCC CGG GAG GC G GCA GCG TGA GTA CCT TCA C AC GTC CCA TGC GCC GTG CTG T
Tau60-1A	CA AAC ACG TCC CGG GAG GCG GCA ATG TGA GTA CCT TCA C AC GTC CCA TGC GCC GTG CTG T
Tau60-2G	CA AAC ACG TCC CGG GAG GCG GCG GTG TGA GTA CCT TCA C AC GTC CCA TGC GCC GTG CTG T
Tau19-WT	GCA GTG TGA GTA CCT TCA C
Tau19-0C	GCA GCG TGA GTA CCT TCA C
Tau19-1A	GCA ATG TGA GTA CCT TCA C
Tau18_WT	GCA GTG TGA GTA CCT TCA
Tau18_0C	GCA GCG TGA GTA CCT TCA
Tau18_1A	GCA ATG TGA GTA CCT TCA
CVD60_WT	TGC CAG CCA TTC TAG CAG GAG AAGT TCG TTT ACT GCT GCC TGG A G TTG AAT TTC TTG AAC
CVD60_1C	TGC CAG CCA TTC TAG CAG GAG AAGT TCG CTT ACT GCT GCC TGG A G TTG AAT TTC TTG AAC
CVD60_0G	TGC CAG CCA TTC TAG CAG GAG AAGT TCG TGT ACT GCT GCC TGG A G TTG AAT TTC TTG AAC

SNV sites are in red; underlined are the fragments complementary to P and R strands; RNA nucleotide are shown in low cases.

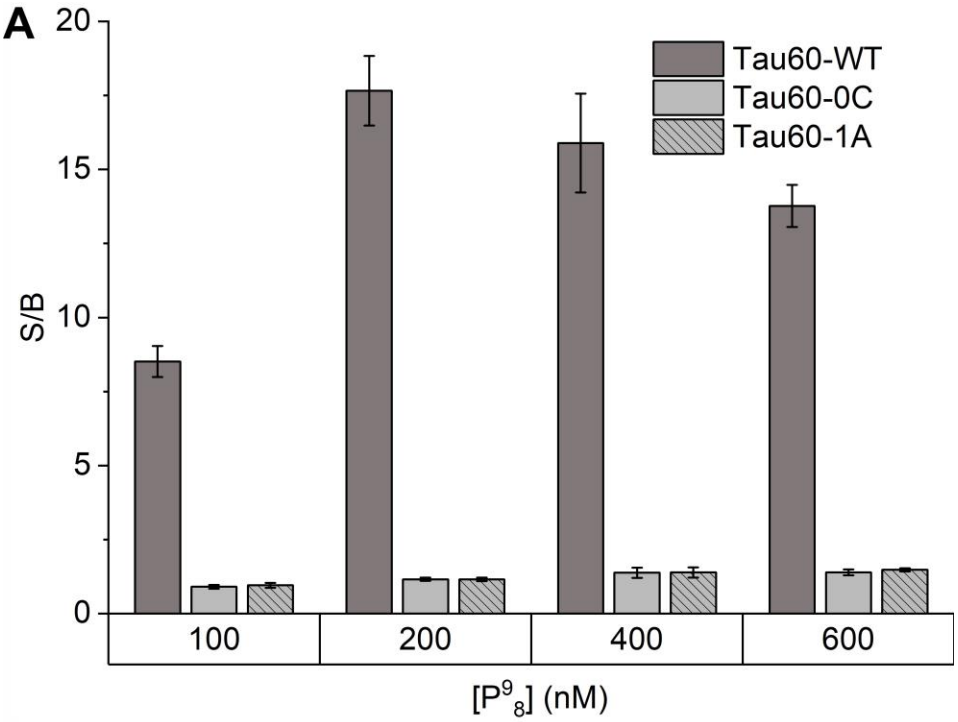

B

	S/B			D_f	
[P^9_8] (nM)	**WT**	**0C**	**1A**	**0C**	**1A**
100	8.5	0.9	1.0	1.01	1.00
200	17.7	1.2	1.2	0.99	0.99
400	15.9	1.4	1.4	0.97	0.97
600	13.8	1.4	1.5	0.93	0.82

Figure S1. Optimization of P-strand concentration for the OWL2 sensor equipped with P^9_8. A) Response of the sensor containing different concentrations of P^9_8 and 100 nM other sensor's components. B) Table depicting the exact values for S/B from the graph, as well as differentiation factor calculated as $D_f = 1-\Delta F_{mm}/\Delta F_{m,}$ where ΔF represents the difference between the signal and the blank for the mismatched (mm) and matched (m) analyte, respectively.

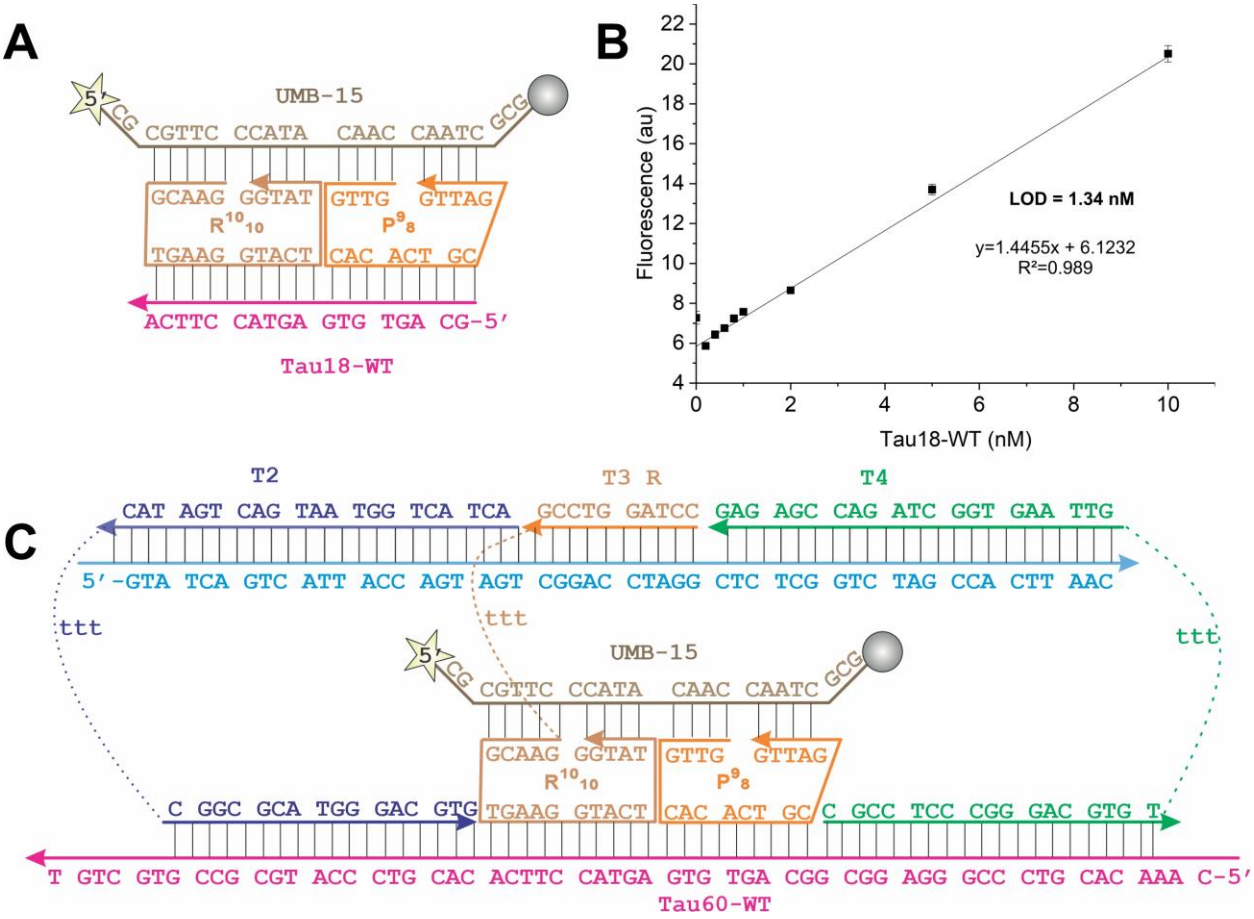

Figure S2. OWL1 and OWL2 sensors in complex with Tau analyte and LOD for the OWL1 sensor. A) OWL1 design consists of R- and P-strand along with UMB-15 to form a complex with a short Tau18-WT analyte. B) Limit of detection for the OWL1 sensor using Tau18-WT. C) OWL2 design has additional T2- and T4- unwinding arms which allow for the opening of a longer Tau60-WT analyte forled into a stable secondary structure.

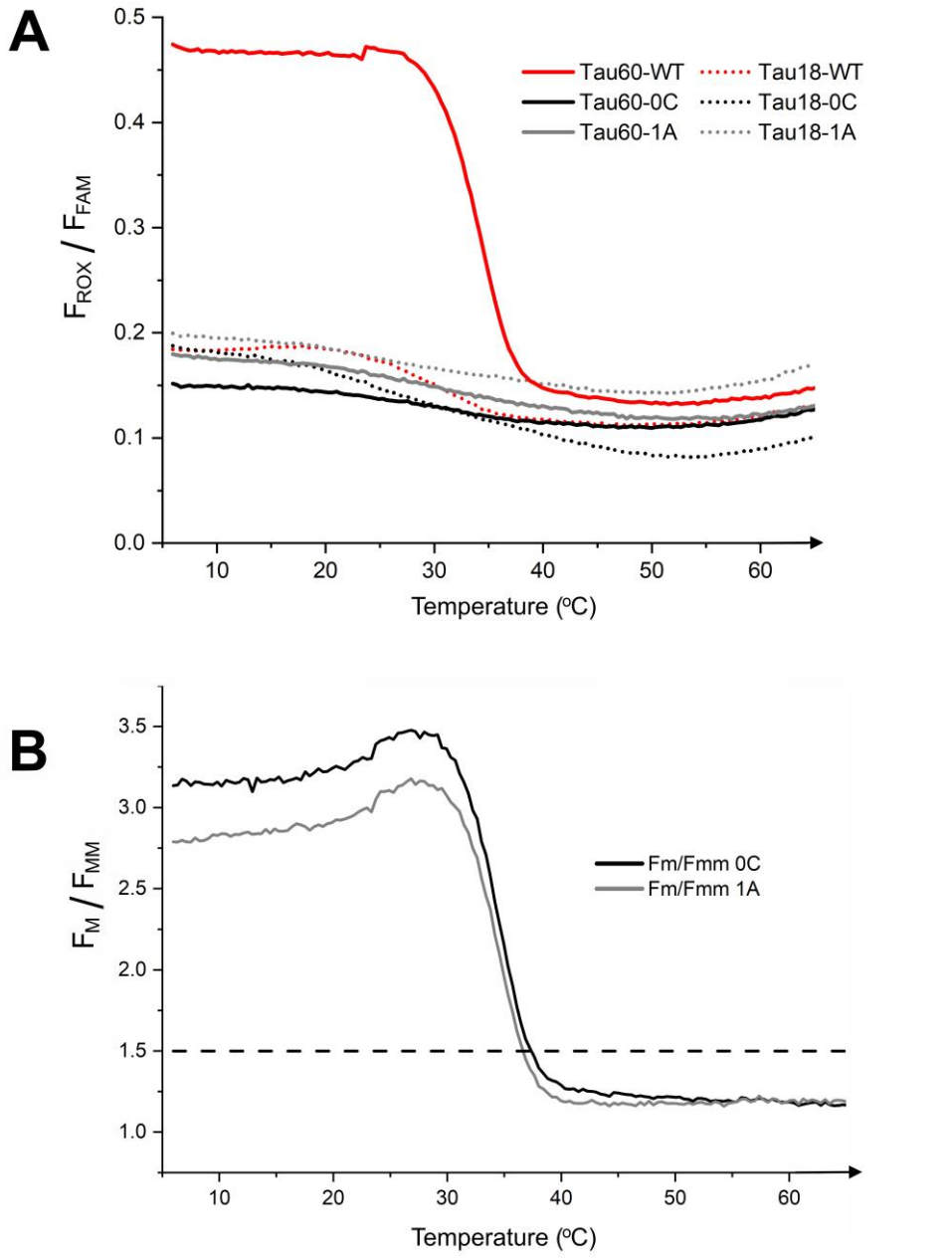

Figure S3. Melting curve for the OWL2 sensor shows differentiation between the fully matched and SNV-containing analytes over a temperature range of 5-38 °C. A. The melting curve normalized using ROX as an internal reporter shows a higher signal triggered by Tau60-WT than by unstructured Tau18-WT, which correlateds to the data in Figure 3B. B. The ratio of the OWL2 sensor's signal triggered by the fully matched Tau60-WT analyte to the signal in the presence of the indicated mismatched Tau60 analyets. The dashed 1.5 line is the threshold at which we determine that the wild-type analyte has been differentiated from the mutant.

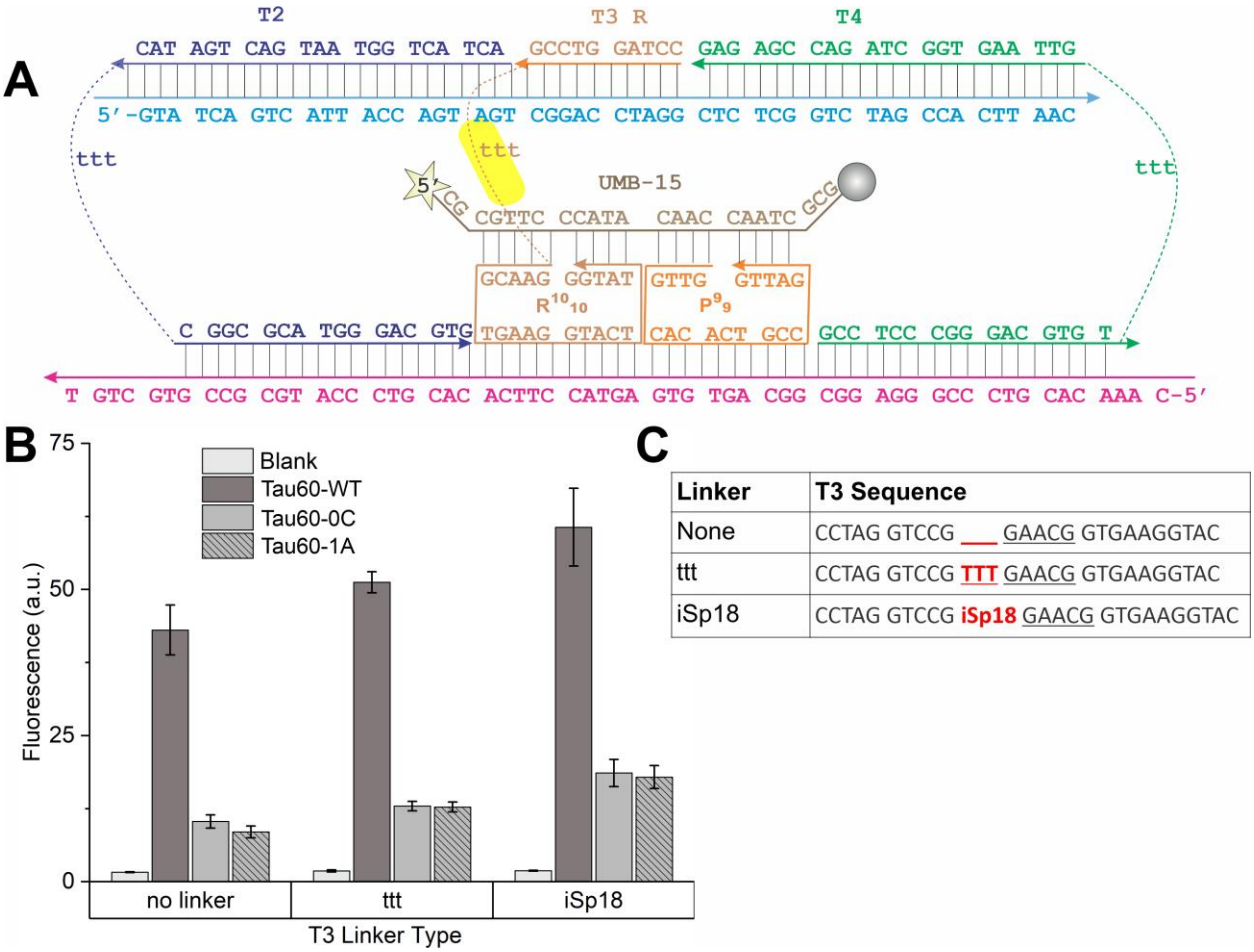

Linker	T3 Sequence
None	CCTAG GTCCG ___ GAACG GTGAAGGTAC
ttt	CCTAG GTCCG TTT GAACG GTGAAGGTAC
iSp18	CCTAG GTCCG iSp18 GAACG GTGAAGGTAC

Figure S4. Flexible linkers between the R stand and scaffold enable higher analyte-triggered signal. (A) OWL2 design with P^{9}_{9} with the highlighted region representing the linker between T1-hybridizing portion of T3 and the UMB- and analyte- hybridizing portion of T3 (B) Fluorescence measured on PerkinElmer Fluorimeter showing an increase in fluorescence for all analytes when flexible linkers were introduced in the T3 strand. (C) Table containing the sequence of T3 and the types of linkers tested.

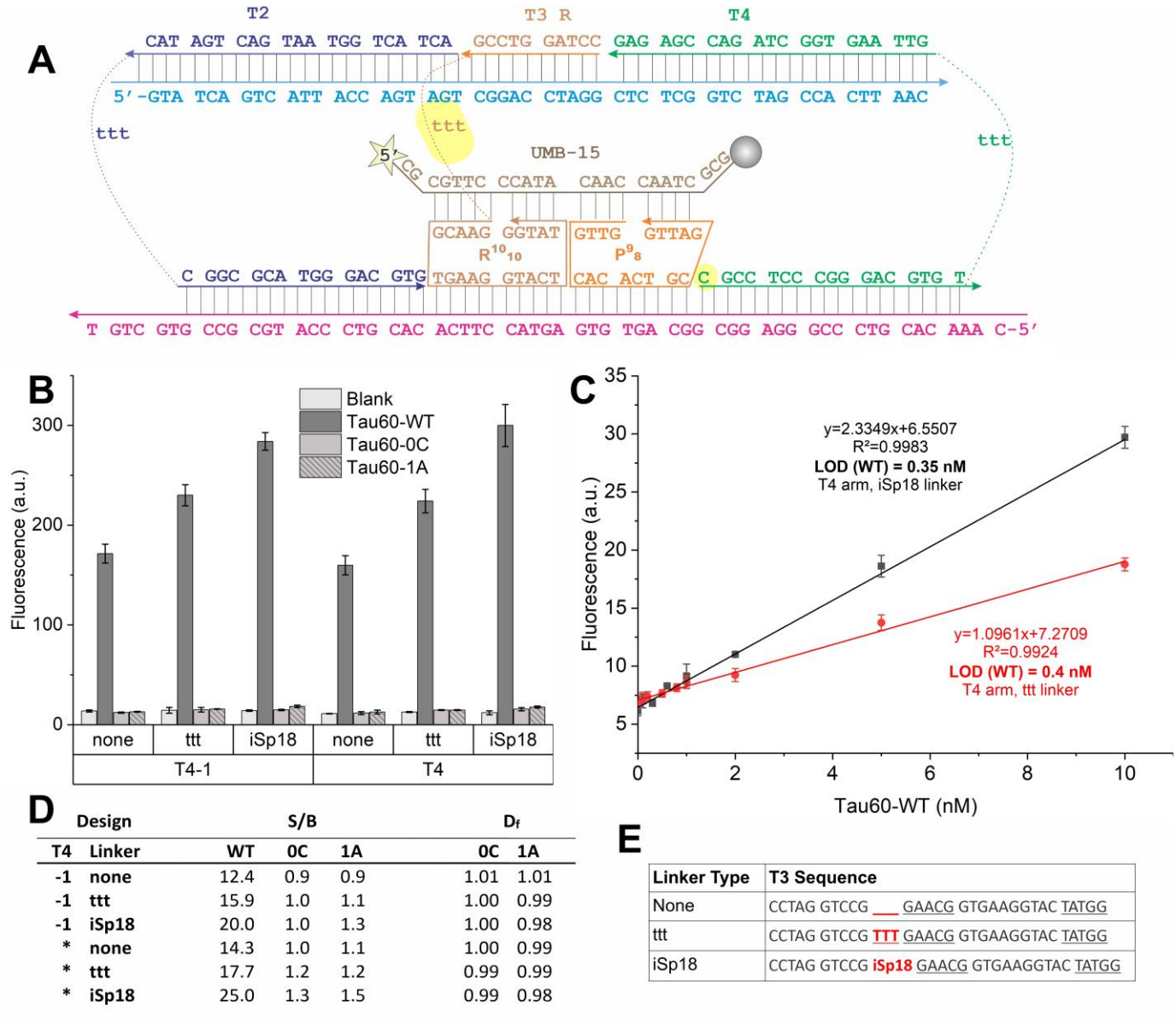

D

Design		S/B			D_f	
T4	Linker	WT	0C	1A	0C	1A
-1	none	12.4	0.9	0.9	1.01	1.01
-1	ttt	15.9	1.0	1.1	1.00	0.99
-1	iSp18	20.0	1.0	1.3	1.00	0.98
*	none	14.3	1.0	1.1	1.00	0.99
*	ttt	17.7	1.2	1.2	0.99	0.99
*	iSp18	25.0	1.3	1.5	0.99	0.98

E

Linker Type	T3 Sequence
None	CCTAG GTCCG ___ GAACG GTGAAGGTAC TATGG
ttt	CCTAG GTCCG **TTT** GAACG GTGAAGGTAC TATGG
iSp18	CCTAG GTCCG **iSp18** GAACG GTGAAGGTAC TATGG

Figure S5. Introduction of a gap between P^9_8 and the T4 analyte-binding arm does not significantly destabilize the OWL structure. Two variations of the T4 strand were used; one hybridizing to the target adjacent to P^9_8 with no gap(denoted with an asterisk), and one, in which there was a gap (denoted as T4-1) between P-strand and T4. **(A)** Design of OWL2 in complex with Tau60-WT, P^9_8, and UMB. The linker variation is highlighted region on T3 R. The highlighted nucleotide in T4 represents the nucleotide that is removed to introduce a gap between P-strand and T4 (T4-1). **(B)** The fluorescent readout from PerkinElmer LS55 Fluorimeter showing that a more flexible linker leads to a higher signal with insignificant compromise to differentiation. **(C)** The limit of detection for the OWL2 sensor with iSp18 linker and T4 arm is 0.35 nM, which is comparable to the 0.4 nM LOD for the ttt linker. **(D)** Signal to background and Differentiation factor for the OWL2 variations shown in (B). **(E)** T3 sequences corresponding to the different linkers.

The LOD for the OWL2 sensor using the folded Tau60-WT was ~0.4 nM (Figure S5,C),

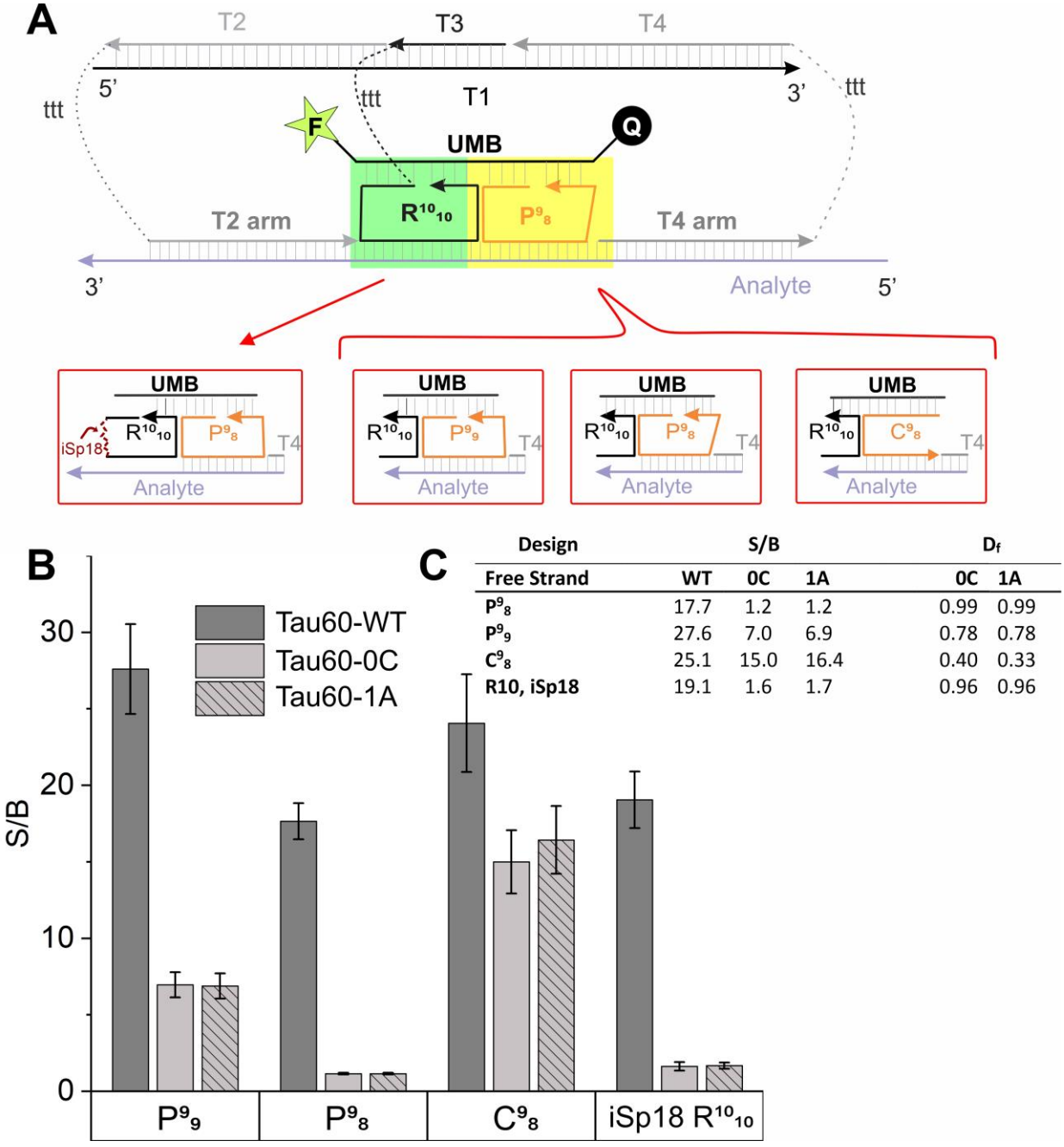

Design	S/B			D_f	
Free Strand	WT	0C	1A	0C	1A
P^9_8	17.7	1.2	1.2	0.99	0.99
P^9_9	27.6	7.0	6.9	0.78	0.78
C^9_8	25.1	15.0	16.4	0.40	0.33
R10, iSp18	19.1	1.6	1.7	0.96	0.96

Figure S6. Constrained structure of the P strand contributes to high selectivity of the OWL2 Sensor. (A) OWL2 design with changes in the highlighted region depicted below the OWL2 structure. R^{10}_{10} with an internal iSp18 linker was used in conjunction with P^9_8, which contains 9 nt complementary to UMB and 8 nt complementary to the analyte. P^9_9 contains 9 nt complementary each to both UMB and analyte. C^9_8 has similar binding to P^9_8, but nucleotides complementary to UMB are consecutive starting at the 5'- end, and the nucleotides complementary to the analyte are consecutive ending at the 3'- end. (B) Tau60-WT-triggered fluorescence for the sensor containing P^9_9 is higher than in case of P^9_8 but has diminished differentiation of mutations. Fluorescence for the sensor with C^9_8 is comparable to that of P^9_9-containing sensor but has poorer differentiation due to the flexibility of the C-strand.

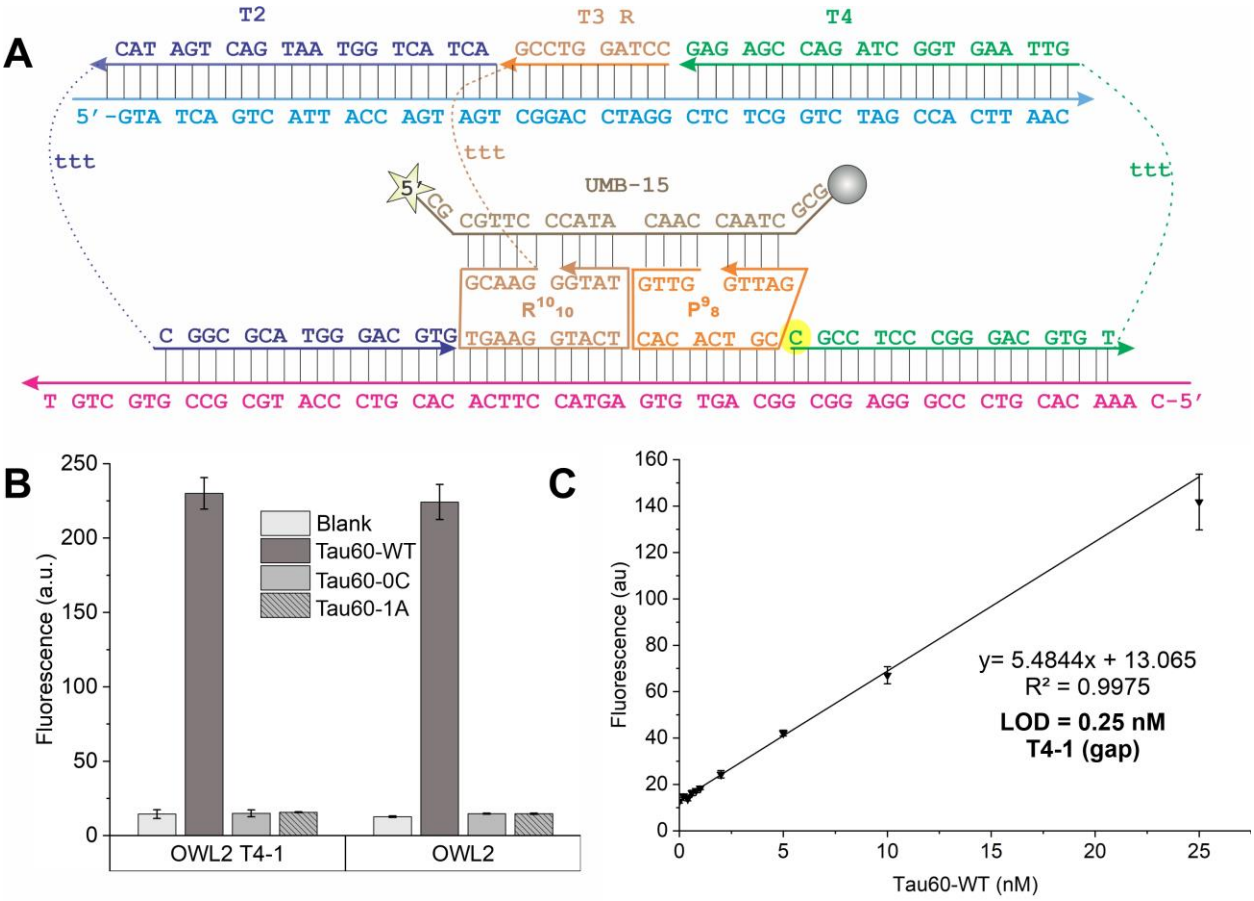

Figure S7. Removal of a nucleotide on T4 to introduce a gap between P and T4 has little effect on fluorescence or limit of detection. (A) OWL2 Design in complex with UMB, $P^{9}{}_{8}$, and analyte. Removed nucleotide on T4 is highlighted in yellow (B) Fluorescence measured on PerkinElmer LS55 Fluorimeter with no appreciable difference between the two designs. (C) Limit of Detection measured for T4-1 (removed nucleotide- a gap is introduced).

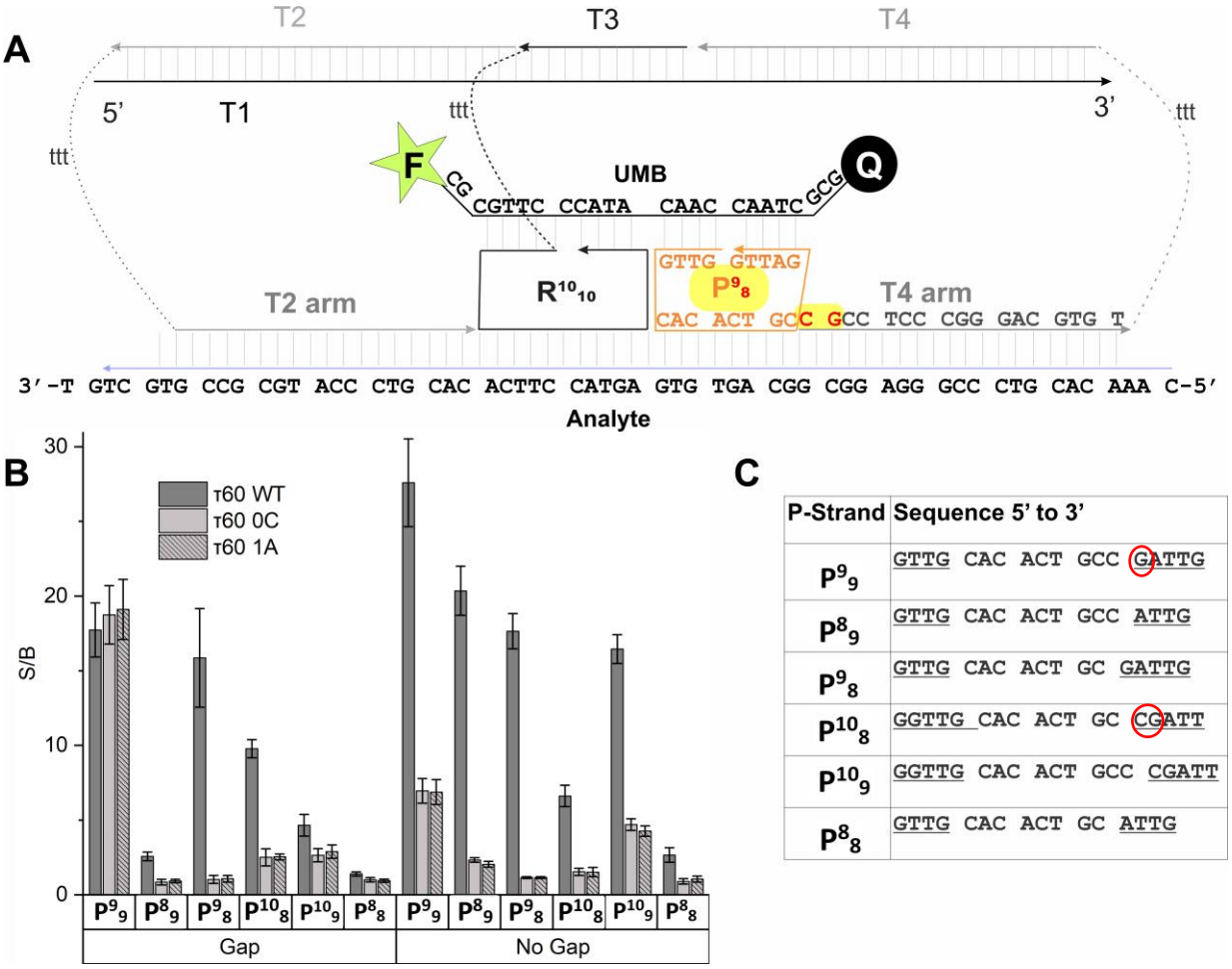

P-Strand	Sequence 5' to 3'
$P^{9}{}_{9}$	GTTG CAC ACT GCC GATTG
$P^{8}{}_{9}$	GTTG CAC ACT GCC ATTG
$P^{9}{}_{8}$	GTTG CAC ACT GC GATTG
$P^{10}{}_{8}$	GGTTG CAC ACT GC CGATT
$P^{10}{}_{9}$	GGTTG CAC ACT GCC CGATT
$P^{8}{}_{8}$	GTTG CAC ACT GC ATTG

Figure S8. Introduction of a single nucleotide gap between the T4 arm and the P strand. **(A)** The gap introduction between the P-strand and T4 arm by shortening the T4 arm by a single nucleotide slightly destabilizes the OWL2 Structure. **(B)**. S/B for the fully matched analyte decreases with the gap introduction, except in the case of $P^{10}{}_{8}$. We believe the increase in signal observed for the $P^{10}{}_{8}$.-containing sensor with the gap is due to the sequence of the P-strand: when the gap is present, the first nucleotide of the 3'-terminal UMB-binding arm that is intended to hybridize with UMB, circled in panel C, may instead hybridize with the analyte since they share complementarity.

We exposed the OWL2 sensor to the effect of a single nucleotide gap between the P-strand and T4-arm and observed that the gap introduction caused a decrease in S/B for all variations of the P-strand, except for $P^{10}{}_{8}$ (Figure S5, S8, Table S4). When designed with a gap, we found a decrease in S/B from ~17 to ~5 and from ~20 to ~3 WT for the $P^{10}{}_{9}$ and $P^{8}{}_{9}$ -equipped sensors, respectively.

The decrease in signal for $P^{10}{}_{9}$ and $P^{8}{}_{9}$ was explained as a function of the P-strand, UMB, and analyte sequence. When a gap is present between the T4- arm and the P-strand, the first nucleotide of the 3'-terminal UMB-binding arms of the P-strand, designed to hybridize with UMB, is free to fill the gap and hybridize with the analyte instead, thus decreasing the nt complementary to UMB and, consequentially, the signal. Conversely, for $P^{10}{}_{8}$, the same mechanics of the gap-filling nt apply but it instead leads to a signal increase due to enough nt still hybridized with UMB and an increase in analyte-hybridized nts. In all cases, having fewer than 8 nts complementary to UMB leads to a low signal. Overall, $P^{9}{}_{8}$ was the best performing P-strand and was not significantly affected by the presence of a gap.

Table S5. Signal-to-background ratio (S/B) and differentiation factor (D_f) for all analytes with varying combinations of the P-strand and either a 1-nt gap or no gap present.

Design		S/B			D_f	
Gap	**P-strand**	**WT**	**0C**	**1A**	**0C**	**1A**
+	$P^{9}{}_{9}$	17.7	18.8	19.1	-0.06	-0.08
+	$P^{8}{}_{9}$	2.6	0.9	0.9	1.09	1.05
+	$P^{9}{}_{8}$	15.9	1.0	1.1	1.00	0.99
+	$P^{10}{}_{8}$	9.8	2.5	2.5	0.83	0.82
+	$P^{10}{}_{9}$	4.7	2.7	2.9	0.55	0.48
+	$P^{8}{}_{8}$	1.4	1.0	0.95	1.06	1.06
-	$P^{9}{}_{9}$	27.6	7.0	6.9	0.78	0.78
-	$P^{8}{}_{9}$	20.4	2.3	2.0	0.93	0.95
-	$P^{9}{}_{8}$	17.7	1.2	1.2	0.99	0.99
-	$P^{10}{}_{8}$	6.6	1.5	1.5	0.90	0.91
-	$P^{10}{}_{9}$	16.5	4.7	4.3	0.76	0.79
-	$P^{8}{}_{8}$	2.7	0.9	1.1	1.06	0.96

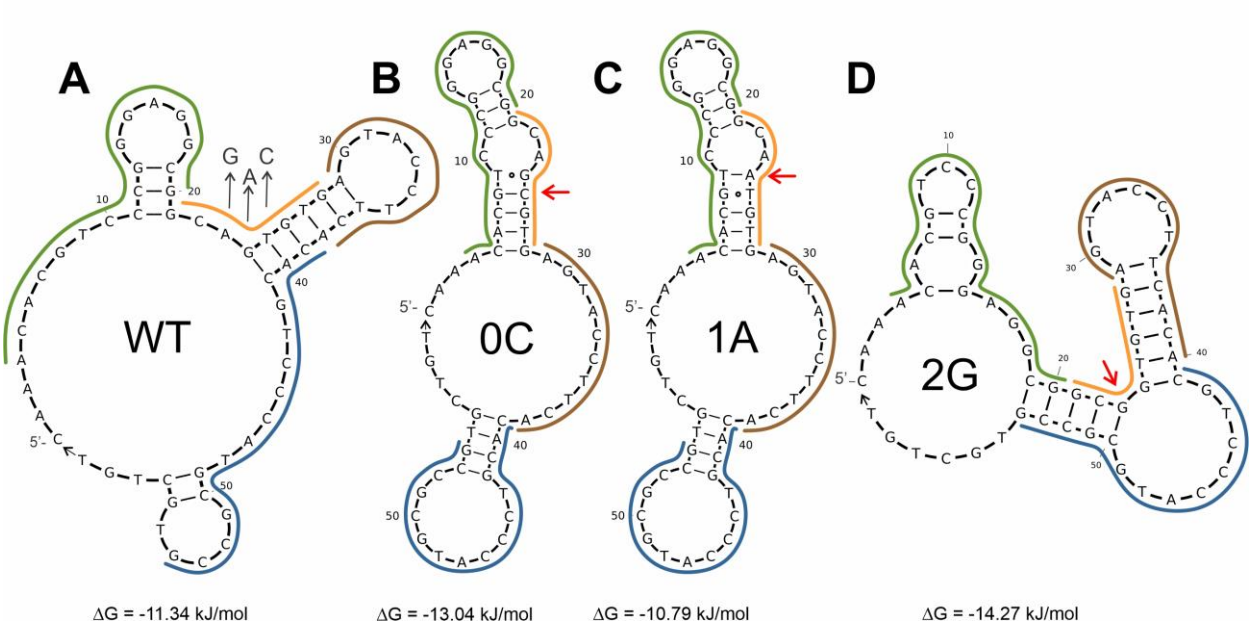

Figure S9. Predicted secondary structures and free energies of the Tau analytes. (A) Tau60-WT with T2-binding arms outlined in blue, T3-R-binding in brown, P- binding in orange, and T4-binding in green. SNV in the mutant analytes - 0C (B), 1A (C), and 2G (D) -are indicated with a red arrow.

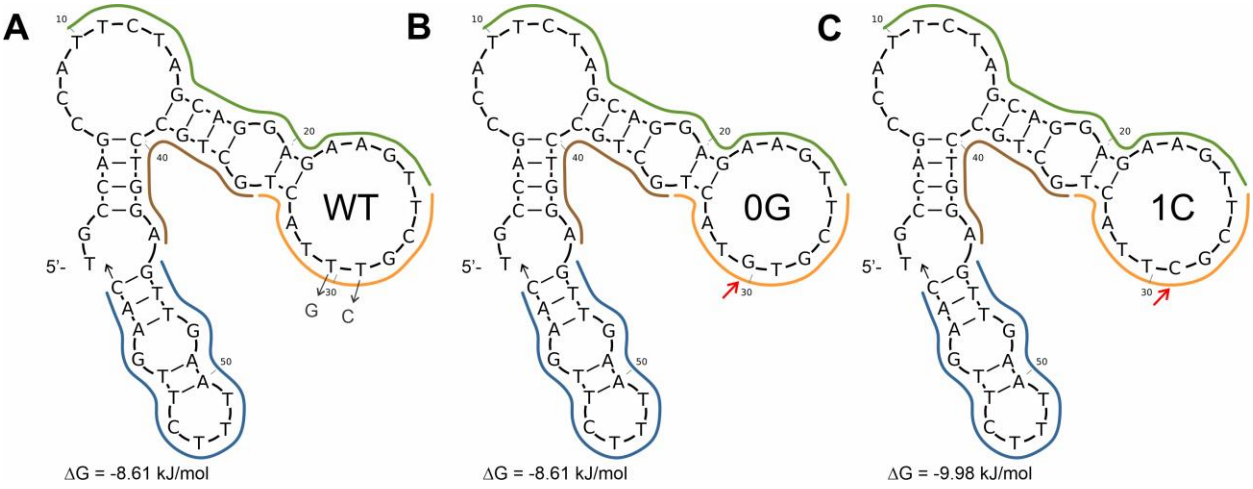

Figure S10. Predicted secondary structures and free energies of the Covid-19 analytes. (A) CVD60-WT with T2-binding portions highlighted in blue, T3-R-binding in brown, P- binding in orange, T4-binding in green, and SNV-locations indicated by arrows. (B) and (C) SNV-containing mutants CVD60-0G and CVD60-1C with mutation positions indicated by red arrows.

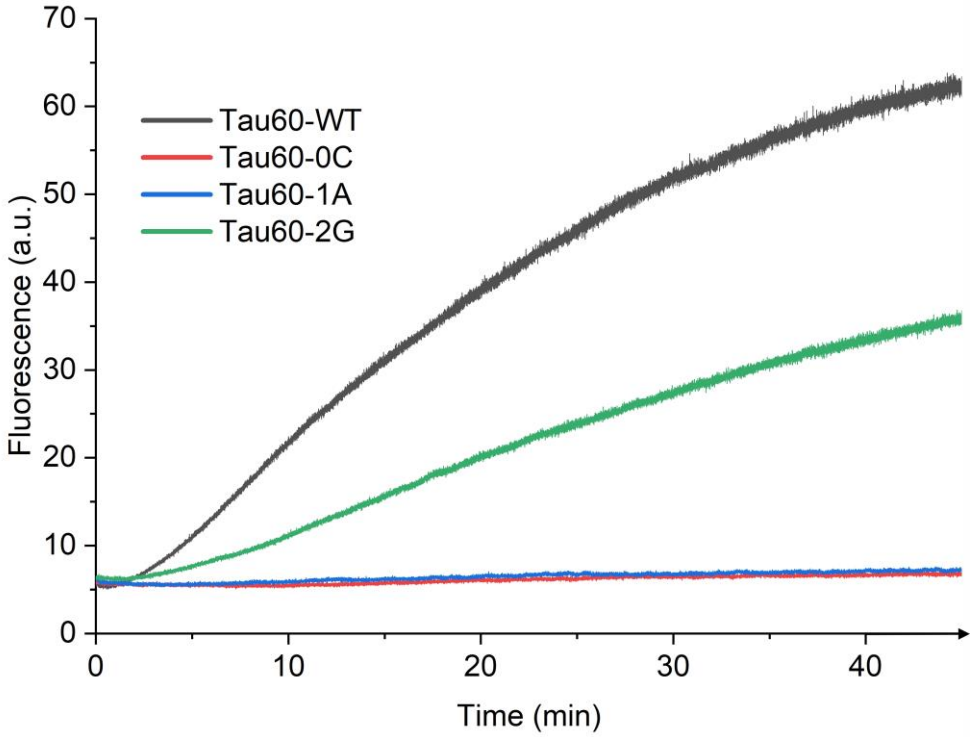

Figure S11. *F*luorescent response of the OWL2 sensor triggered by the Tau analytes over time for A four-fold increase in fluorescence can be seen over the first ten minutes in case of Tau60-WT with discrimination against mutants 0C and 1A. The 2G mismatch shows a slower signal increase when compared to the WT.

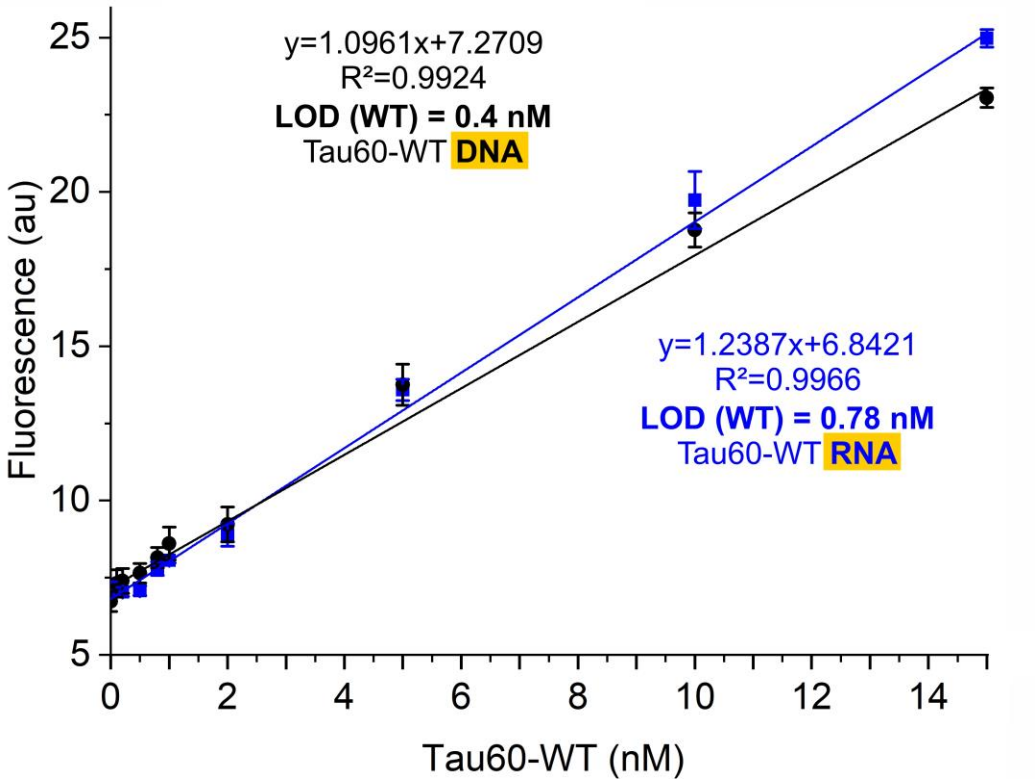

Figure S12. Limit of detection for Tau60-WT DNA and RNA using the OWL2 sensor with P^{9}_{8} in buffer 1. LOD for the DNA sequence (black) was found to be 0.4 nM, and LOD for the RNA sequence (blue) (Table S3) was found to be 0.78 nM. Since the disease-causing SNV-containing analyte is Tau60 mRNA, this provides evidence that the OWL2 sensor would be applicable to real-world analysis.